

# Synthesis of flexible free-standing silver nanoparticles-graphene films and their surface-enhanced Raman scattering activity

Nan Zhao · Xiaonong Cheng · Yazhou Zhou ·  
Mingxin Yang · Juan Yang · Tao Zhong ·  
Sihui Zheng

Received: 26 October 2013 / Accepted: 19 February 2014 / Published online: 13 March 2014  
© Springer Science+Business Media Dordrecht 2014

**Abstract** A free-standing and flexible silver nanoparticles-graphene (Ag NPs-GE) film with high surface-enhanced Raman scattering (SERS) sensitivity has been developed. First, the high stable and dispersive Ag NPs-GE composite was fabricated by in situ reduction using graphene oxide sheets as substrates and the hydrazine hydrate as a reducing agent in the solvothermal environment. Second, the Ag NPs-GE films can be fabricated through vacuum filtration of the Ag NPs-GE suspension. Transmission electron microscope (TEM) images show that the Ag NPs with an average size of 22 nm and a narrow

particle size distribution are uniformly distributed on GE sheets. The coverage density of Ag NPs onto the surface of GE sheets can be successfully controlled by tuning the concentration of silver ion precursor. As-prepared Ag NPs-GE substrates have good SERS sensitivity due to the high SERS-active of Ag NPs. The enhancement factor for  $1 \times 10^{-6}$  M of rhodamine 6G molecules adsorbed onto the surface of substrate is about  $2.7 \times 10^5$ . The SERS activity toward crystal violet and *Escherichia coli* was also investigated.

**Keywords** Graphene · Silver nanoparticles · Surface-enhanced Raman scattering · Rhodamine 6G · Two-dimensional materials

**Electronic supplementary material** The online version of this article (doi:10.1007/s11051-014-2335-0) contains supplementary material, which is available to authorized users.

N. Zhao · X. Cheng · Y. Zhou · J. Yang ·  
T. Zhong · S. Zheng  
School of Materials Science and Engineering, Jiangsu  
University, 301 Xuefu Road, Zhenjiang 212013,  
People's Republic of China  
e-mail: zhaonan@ujs.edu.cn

X. Cheng  
e-mail: xncheng@mail.ujs.edu.cn

Y. Zhou  
e-mail: zhouyazhou60@gmail.com

T. Zhong  
e-mail: 362403961@qq.com

S. Zheng  
e-mail: 893741858@qq.com

M. Yang  
Jingjiang College of Jiangsu University, 301 Xuefu Road,  
Zhenjiang 212013, People's Republic of China  
e-mail: 982448230@qq.com

J. Yang (✉)  
Key Laboratory of Soft Chemistry and Functional  
Materials, Nanjing University of Science and Technology,  
Ministry of Education, Nanjing 210094,  
People's Republic of China  
e-mail: yangjuan6347@mail.ujs.edu.cn

## Introduction

Since the surface-enhanced Raman scattering (SERS) has been unexpectedly discovered in 1974 by Fleischmann et al. (1974), it has inspired a worldwide effort to explore its mechanism both theoretically and experimentally. Usually, due to the strong surface plasmon resonance of the metal nanoparticles (normally gold or silver nanoparticles, i.e., Au NPs or Ag NPs), metal substrates, either with rough surfaces or in the form of nanoparticles, can be used as SERS substrates with enhancement factors (EF) as large as  $10^{10}$ – $10^{15}$  (Jeanmaire and VanDuyne 1977; Albrecht and Creighton 1977; Kneipp et al. 1999). With the development of nanofabrication and the understanding of the plasmonic properties of metal substrates in recent years, the SERS has become a useful technique in surface chemistry and physics because of its high sensitivity and the potential of in situ detection of biomaterials and hazardous components in fluids, which not only for human health and safety, but also for environmental and industrial applications (Kim et al. 2012).

Novel substrates based on noble metal nanoparticles have high sensitivity of SERS, which hold a great promise for fabrication of SERS substrates. However, if SERS is to be used readily in routine procedures, the substrates need to be cheap, stable, and reusable so that they can be stored for long lengths of time between measurements (Hasell et al. 2008). Due to the high manufacturing cost and low stability of noble metal SERS substrates, designing and assembling of low manufacturing cost, highly effective and stable substrates for SERS application still requires further improvement (Abu Hatab et al. 2008). Recently, series new class of SERS substrates have been fabricated, where metal nanoparticles are embedded into inorganic or polymer substrates. For example, Hasell et al. reported the Ag NPs-impregnated polycarbonate (Ag NPs-PC) substrates (2008) and He et al. reported the Ag NPs-poly(vinyl alcohol) (Ag NPs-PVA) (He et al. 2009). Kneipp et al. have observed SERS of single-walled carbon nanotubes in contact with fractal silver colloidal clusters with an enhancement of approximately 12 orders of magnitude (2000). Graphene (GE) has an analogous structure to carbon nanotubes, and it is expected to show a similar SERS effect.

GE possesses a special two-dimensional crystalline structure, large specific surface area, remarkable electrical conductivity, excellent adsorptivity, high

chemical and thermal stability; and has become one of the most famous stars to fabricate graphene-based composite material as a “substrate” at present (Lu et al. 2012). Particularly for fabrication Ag NPs-GE composites, GE used as substrate can prevent the Ag NPs from aggregation. The new class of Ag NPs-GE composites have shown great promising applications in electronics, optics, sensors, and biomaterials (Yang et al. 2011; Xu and Wang 2009), especially in SERS substrates. For example, Fu et al. have reported the fabrication of silylated graphene oxide (GO) sheets sandwiched between colloidal Ag NPs and silver piece, which can be used as SERS substrate (2010); Kamat et al. have designed the reduced graphene oxide-Ag nanoparticle (RGO-Ag NP) composite to boost SERS sensitivity of a porphyrin derivative (Murphy et al. 2013). However, the sensitivity of these SERS materials remains to be improved.

In our previous work, Ag NPs can be assembled onto the GE sheets to form Ag NPs-GE composites through the solvothermal method, which showed excellent electrical conductivity (Yang et al. 2011). In fact, GE-based sheets are very pliable and can be processed facilely into paper-like and flexible materials, which can make the Ag NPs-GE become the free-standing and flexible SERS substrates (Dikin et al. 2007).

Thus, in this paper, we demonstrated a class of large-scale, portable, stable, flexible, free-standing and inexpensive SERS substrates. First, the high stable and dispersive Ag NPs-GE aqueous solution was prepared by solvothermal method using GO sheets as substrates and the hydrazine hydrate as a reducing agent. Then, through the vacuum filtration, the Ag NPs-GE film can be obtained. The SERS effects of the obtained substrates was also investigated in detail with rhodamine 6G (R6G), crystal violet (CV), and bacterial cell such as *Escherichia coli* (*E. coli*) as the target molecules.

## Materials and methods

### Materials

GO was synthesized from purified natural graphite bought from Shanghai Yifan Company with a mean particle size of 1.5  $\mu\text{m}$  according to the method reported by Hummers and Offeman (1958). Analytical-grade reagents, including silver acetate (AgAC), hydrazine hydrate, R6G, and CV were purchased from

Shanghai Chemical Reagent Corporation and used as received.

### Synthesis of Ag NPs–GE composite

The synthesis of Ag NPs–GE nanocomposite involved two steps, according to a modified process described in our previous work (Yang et al. 2011). In the first step, GO (50 mg) was dispersed in the ethanol solution (50 mL) with sonication for 2 h, and the AgAC ethanol solution (5 mg mL<sup>-1</sup>, 10 mL) was added into the GO ethanol solution with sonication for 2 h. The mixture was centrifuged and washed copiously with ethanol. The obtained sample was dried in a vacuum at 30 °C for 8 h and labeled as Ag<sup>+</sup>–GO. In the second step, 25 mg of Ag<sup>+</sup>–GO composite was mixed with 25 mL de-ionized water and 50 µL hydrazine, under sonication for 1 h, and the resulting mixture was transferred into 25-mL stainless steel Teflon-lined autoclave. The autoclave was sealed, kept at 140 °C for 40 min, and then naturally cooled to room temperature. After the reaction, the solution was centrifuged, washed with de-ionized and ethanol water three times each, dried overnight in vacuum at 30 °C, and the Ag NPs–GE composite were obtained.

### Synthesis of Ag NPs–GE composite film

For film preparation, the Ag NPs–GE was dispersed in water with sonication at a concentration of 0.1 mg mL<sup>-1</sup>. The diluted suspension was vacuum filtrated using a mixed cellulose ester membrane with 25 nm pores (Millipore). The film was allowed to be dried in vacuum at 30 °C. The as-prepared films were thermal annealing reduced, if necessary, in a tube furnace at 300, 500, and 700 °C under H<sub>2</sub>/Ar atmosphere (volume ratio = 1/5) for 2 h and cooled naturally to room temperature.

### Characterization

The optical property of nanocomposites was tested on a Shimadzu UV-2550 spectrophotometer at room temperature. The crystal structure of the composites was characterized by a Philips 1,730 powder X-ray diffractometer (XRD) with Cu K $\alpha$  radiation ( $\lambda = 1.5406 \text{ \AA}$ ). The morphology and microstructures were observed by a JEOL 2011 transmission electron microscope (TEM) at an accelerating voltage of 200 kV. The surface images of film were conducted on a JEOL 6460

scanning electron microscope (SEM). Thermogravimetric analysis (TGA) was conducted with a Netzsch Sta449C that was fitted to an air gas at a heating rate of 10 °C min<sup>-1</sup>. The Raman spectra were recorded on a MXR Raman system. The excitation line at 532 or 780 nm provided by an argon ion laser was used at the power of 5 mW and laser spot size of 2.1 µm. The acquisition time for each measurement was 10 s. Replicate measurements of three times on different areas were made to verify that the spectra were true representations of each experiment. The relative standard deviation is within 5 % based on the strongest peak intensity of R6G/CV on the Raman spectrum.

### Preparation of sample for Raman measurement

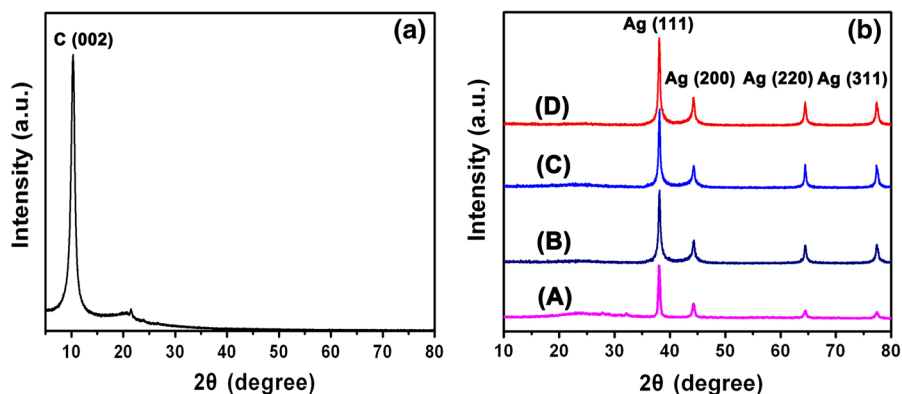
For Raman measurement with R6G and CV as target molecules, the samples were prepared according to the procedure described in the literature (Fu et al. 2009). To record the Raman spectrum of R6G/CV molecules adsorbed on Ag NPs–GE substrates, the above substrates were first immersed into 5 mL ethanol. Then, an aliquot of 10 µL of R6G/CV (10<sup>-4</sup> M) was added to the solution and it was stirred carefully at 20 °C for 12 h. Finally, it was washed thoroughly with ethanol to remove unbound R6G/CV molecules and dried at room temperature to evaporate all of the ethanol.

For Raman measurement with *E. coli* as target molecule, *E. coli* cells were first grown in 5 mL of LB (Sigma) broth (~5 h) to an OD<sub>600</sub> = ~1, washed five times with water, and resuspended in 0.25 mL of water. Then, about 1 µL of the bacteria suspension is placed on the Ag NPs–GE composite film using a loop. The Raman spectrum of bacterial was obtained under the excitation line of 532 nm at the power of 0.5 mW. The acquisition time for each measurement was 10 s. Non-SERS bacterial sample, excited with about 0.1 mW at 532 nm, was correspondingly placed on glass.

## Results and discussion

Hydrazine is used as a highly effective reducing agent to fabricate GE through chemical conversion. Here, hydrazine not only can be used to reduce the GO, but also to reduce the Ag<sup>+</sup> to Ag NPs. Figure 1b shows the XRD patterns of the Ag NPs–GE composites prepared with different weight ratios of AgAC: GO (3:5, 4:5,

**Fig. 1** XRD patterns of **a** GO powders and **b** Ag NPs-GE composites fabricated under the different weight ratios of AgAC: GO: (A) 3:5, (B) 4:5, (C) 5:5, and (D) 6:5



5:5, and 6:5), where reflections of Ag NPs and GE are identified. The Ag NPs-GE composites show characteristic peaks at  $38.1^\circ$ ,  $44.3^\circ$ ,  $64.4^\circ$ , and  $77.4^\circ$ , which can be assigned to the (111), (200), (220), and (311) planes of the cubic Ag crystal (JCPDS No. 04-0783). In addition, the intensity of Ag became higher with the increase of weight ratios of AgAC: GO. However, no obvious diffraction peaks of GO (Fig. 1a) were observed in the as-synthesized composites. We conclude that the content of Ag NPs is relatively high, and it is possible that the diffraction signals of Ag NPs may cover up those of the carbon sheets. Additionally, no peaks corresponding to impurities were detected. So, it can be concluded that a kind of Ag NPs-GE composite has been formed.

TGA curves of GO and Ag NPs-GE composites as prepared with the weight ratio of AgAC: GO of 3:5, 4:5, 5:5, and 6:5 are shown in Fig. 2. For GO, in agreement with previous reports in the literature (Kudin et al. 2008), the main mass loss takes place around temperature range of 100–300 °C, corresponding to the decomposition of labile oxygen functional groups present in the material. There is also a mass loss ( $\sim 9\%$ ) below 100 °C, which can be attributed to the removal of adsorbed water. Further, a slower, steady mass loss ( $\sim 53\%$ ) over the whole temperature range between 400 and 600 °C can be assigned to the removal of more stable oxygen functionalities. As for Ag NPs-GE composites fabricated under the weight ratio of 3:5, the total weight loss decreased to  $\sim 60\%$  as shown in Fig. 2. The total weight loss of composites decreased as the increasing of weight ratio of AgAC: GO and the weight loss is 42% under the ratio of 6:5. Considering that silver oxide is remained after

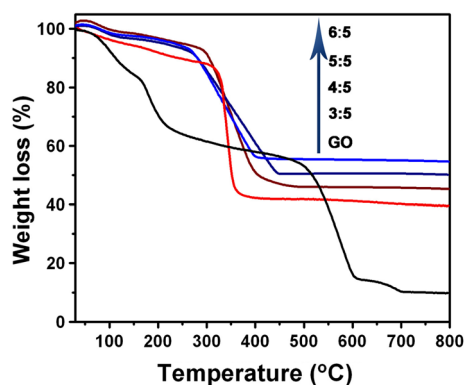


**Fig. 2** TGA data obtained for GO powders and Ag NPs-GE composites fabricated under different weight ratios of AgAC: GO

the TGA experiment, the loading percentage of Ag NPs in this composite can be estimated to be 54 wt% by TGA.

It is well known that the GO sheets bear bulky oxygen-containing functional groups on their basal planes and edges and these functional groups have been used as anchors for the adsorption of positive metal ions (here is  $\text{Ag}^+$ ). The adsorbed silver ions can be reduced to Ag NPs by hydrazine with in situ reduction. Additionally, the oxygen-containing groups on the GO also act as the nucleation center for nanoparticles, which can stabilize the particles after growth. The morphologies of the Ag NPs-GE composites can be observed by TEM. Figure 3a gives the TEM image of Ag NPs-GE composites prepared with the weight ratio of AgAC: GO of 3:5. It can be clearly seen that the almost transparent GE sheets are fully exfoliated and decorated with a few of spherical-like Ag NPs and no obvious aggregation or free Ag NPs are detected. It is well

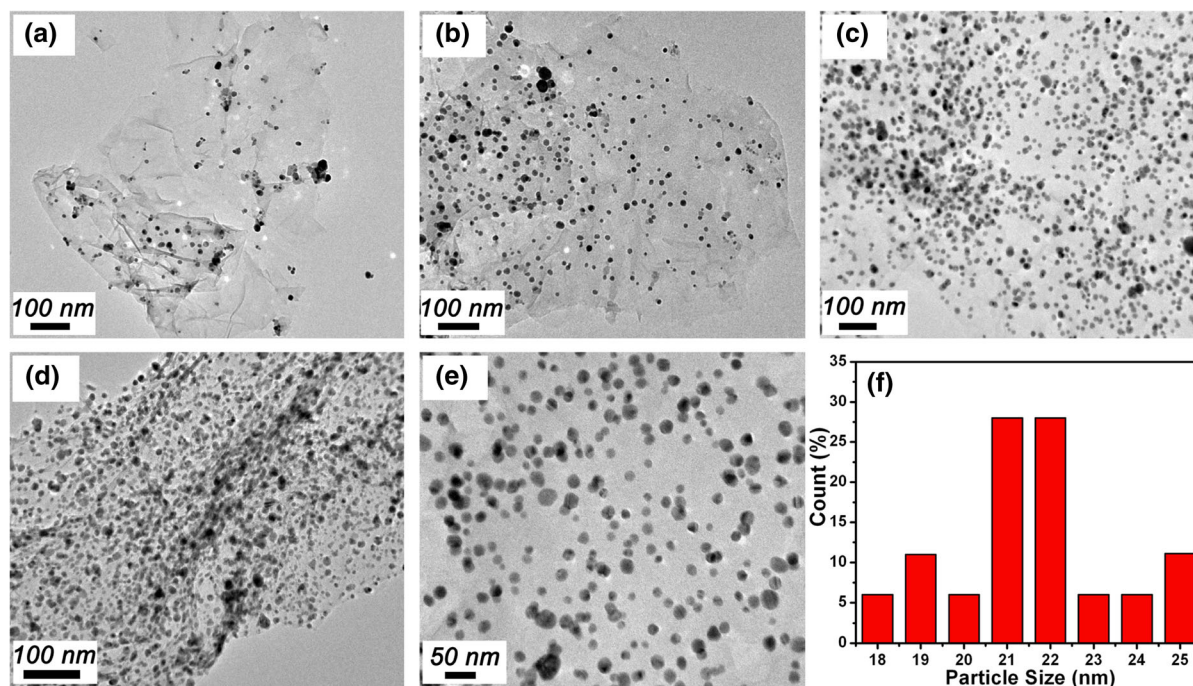


**Fig. 3** Typical TEM images of Ag NPs–GE composites synthesized under the weight ratio of AgAC: GO: **a** 3:5, **b** 4:5, **c** 5:5, and **d** 6:5; **e** HRTEM image of Ag NPs–GE composite of (c); and **f** the particle size distribution for Ag NPs in **e**

known that the decoration of Ag NPs on GE sheets is visibly influenced by the initial weight ratio of AgAC: GO sheets, as shown in Fig. 3a–d. When the ratio was increased to 4:5, in comparison with the weight ratio of 3:5 (Fig. 3a), the higher loading percentage of Ag NPs is shown in Fig. 3b. With the increase of the weight ratio of AgAC: GO sheets (5:5) using more concentrated AgAC solution, more Ag NPs are observed and almost covered the whole GE sheets (Fig. 3c). Figure 3e gives the detailed view of the composite from Fig. 3c, indicated clearly that the Ag NPs of composites have an average particle size of 22 nm with a narrow particle size distribution (Fig. 3f). Furthermore, no aggregated sheets and free NPs are found. However, when the weight ratio of AgAC: GO increases to 6:5, a large quantity of Ag NPs was aggregated seriously due to the saturated concentration. According to the above observations, it is concluded that not only Ag NPs were effectively decorated on GE sheets by this in situ reduction method, but also the coverage density could be successfully controlled by tuning the concentration of silver ion precursor.

The morphology features of Ag NPs–GE composites have also been thoroughly investigated using

SEM. As shown in Fig. 4, for Ag NPs–GE composites prepared with the weight ratio of AgAC: GO of 3:5, a few of Ag NPs can be seen on the surface of GE sheets (Fig. 4a). When the weight ratio of AgAC: GO increased, much more Ag NPs were assembled onto the GE sheets, which can be observed in Fig. 4b–d. More importantly, we found that the NPs also be wrapped with the GE sheets (Fig. 4c). The GE sheets can provide protection of Ag NPs from oxidation in the surrounding environment, which may make the Ag NPs–GE SERS substrates have a high degree of temporal stability. When the weight ratio of AgAC: GO increased to 6:5, a large quantity of Ag NPs was aggregated seriously onto the surface of GE sheets (Fig. 4d). The SEM results are consistent with TEM results.

It is well known that the optical properties of Ag NPs are strongly dependent on their size and shape, which can describe the structure of the composite using the UV–Vis spectra. The UV–vis absorption spectra of Ag NPs–GE composites with different initial mass ratios are shown in Fig. S1 (Supplementary Information). In the UV–vis spectra, the Ag NPs–GE composite exhibits two characteristic absorbance

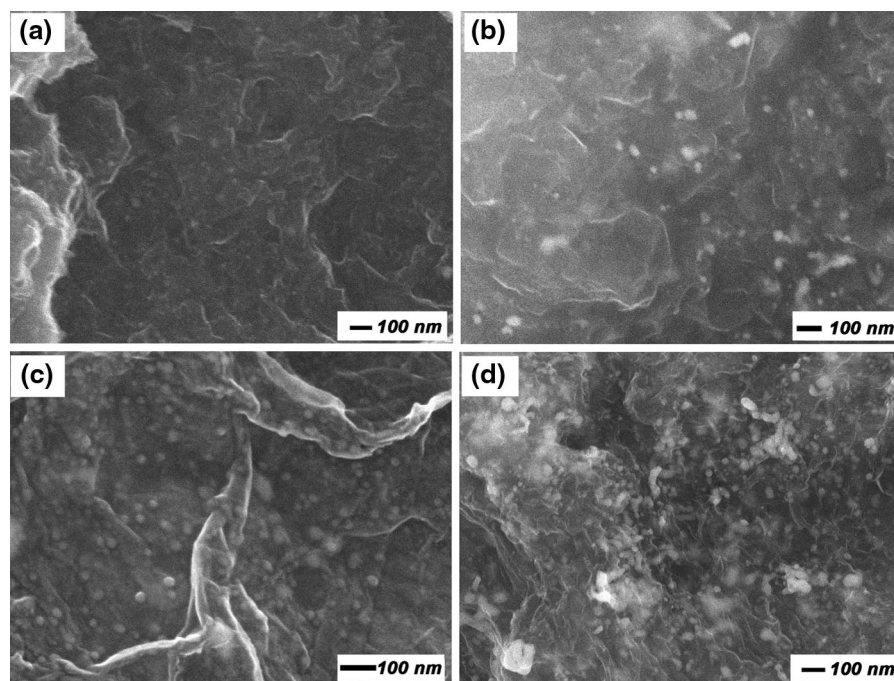


**Fig. 4** Typical SEM images of Ag NPs–GE composites synthesized under the weight ratio of AgAC: GO: **a** 3:5, **b** 4:5, **c** 5:5, and **d** 6:5

peaks. One is near 265 nm, which can be attributed to GO absorption with a great red-shift from 231 nm, suggesting that the electronic conjugation within the GE sheets is restored upon hydrazine reduction. The other absorption peak around 420 nm is attributed to Ag NPs, which was visibly influenced by the initial weight ratio of AgAC: GO. With the increase of loading percentage of Ag NPs in composites, the characteristic absorbance peak became higher. In addition, the full width at half-maximum of Ag NPs in composite was decreased (from 3:5 to 5:5) due to the small size and narrow particle size distribution of the Ag NPs. However, with increase of weight ratio of AgAC: GO to 6:5, the characteristic absorbance peak of Ag NPs in composites has red-shifted from 418 to 423 nm due to the formation of aggregated nanostructures. The UV–vis results are consistent with TEM results.

Although there are large amounts of Ag NPs decorated on the GE sheets, the resulting composite can also be dispersed in water by sonication process, forming a stable suspension probably due to the hydrophilic character of the chemically obtained GE. Figure S2 (Supplementary Information) is the photograph of the aqueous dispersions of the Ag NPs–GE

composites ( $0.1 \text{ mg mL}^{-1}$ ), with few precipitate occurring in the bottom after 24 h at room temperature, indicating its good stability and good dispersion property. Through vacuum filtration of this stable suspension, the Ag NPs–GE film can be prepared. The morphologies of the surface and cross section of the Ag NPs–GE film can be displayed with SEM analysis, as shown in Fig. 5. Figure 5a gives the morphology of the surface and it can be clearly observed that large amounts of Ag NPs assembled on the 2D substrates, which was consistent with the TEM results. Figure 5b shows the SEM image of the cross-section of the film. The restacking of the carbon sheets was ordered, and the fracture edges exhibited a layered structure throughout the entire cross section. More importantly, large amount of NPs can be observed in the whole cross section.

Raman spectra of GO and Ag NPs–GE films (with AgAC: GO weight ratio of 5:5, the filtration volume of 10 mL) are obtained using a confocal microscope employing a diode laser operating at 532 nm with an output power of 5 mW on the sample (see the Supporting Information Fig. S3). The Raman spectrum of GO shows the well-known main groups of bands: the tangential stretching mode (G band) in the

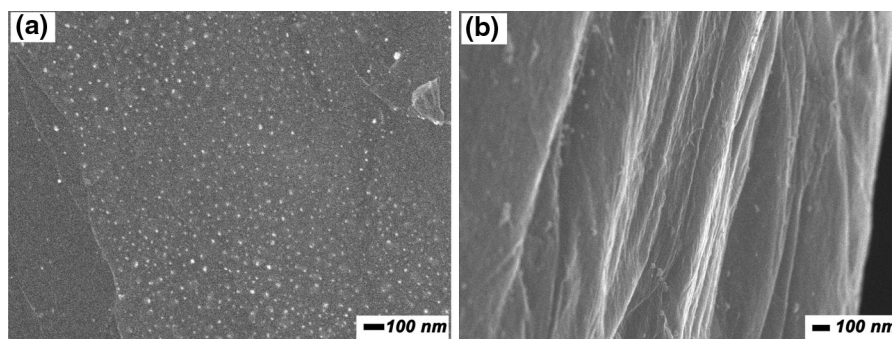


**Fig. 5** Typical SEM images of **a** the surface; and **b** the cross section of Ag NPs–GE film

range of  $1,500\text{--}1,600\text{ cm}^{-1}$  as well as the disorder band (D band) in the range of  $1,200\text{--}1,500\text{ cm}^{-1}$  (Kudin et al. 2008). Interestingly, we noted that the Raman spectroscopy revealed the Raman signal enhancement for Ag NPs–GE film, which was consistent with the SERS effect previously reported in Ag NPs and GO composites (Fu et al. 2010).

R6G, as probing molecule, was chosen as a model target molecule to investigate the SERS activity of Ag NPs–GE film in our system because R6G has distinct Raman features and it is easily to be absorbed on the surface of Ag NPs. Here, the excitation line were changed to 780 nm provided by an argon ion laser. This is because the Raman signals of GE in Ag NPs–GE substrate obtained at 532 nm are much larger than those acquired at 780 nm (see Fig. S3 in supplementary information). The high intensities of D and G bands may cover the characteristic bands of R6G, which makes it difficult to truly reflect the SERS quality of Ag NPs–GE substrate. For comparison, a normal Raman spectrum of R6G in 0.02 methanol solution is obtained. It is apparent that the Raman intensity of pure R6G is very weak (Fig. 6A). However, when the R6G adsorbed onto the surface of Ag NPs–GE substrate (with AgAC: GO weight ratio of 5:5), the intensity of Raman signals for R6G has been remarkably increased, as shown in the spectrum of R6G/Ag NPs–GE (Fig. 6A). The profile of the D band fits a complex band with three main peaks at 1,188, 1,310, and  $1,361\text{ cm}^{-1}$ . Furthermore, we observed that the G band becomes much broader and splits into more bands with full peak shapes ( $1,504$ ,  $1,532$ ,  $1,573$ ,  $1,595$ , and  $1,649\text{ cm}^{-1}$ ). In the region between  $800$  and  $1,700\text{ cm}^{-1}$ , the strong bands in the spectrum of R6G/Ag NPs–GE are the C–C stretching

vibrations at ca.  $1,361$ ,  $1,504$ ,  $1,573$ , and  $1,649\text{ cm}^{-1}$  in SERS spectrum. The Raman peaks are assigned based on proposals in the literatures (Hildebrandt and Stockburger 1984). We note that two strong bands at ca.  $1,131$  and  $1,188\text{ cm}^{-1}$  appeared in the spectrum of R6G/Ag NPs–GE, which can be assigned to the C–H in-plane bend modes, and the bands at ca.  $1,314$  and  $1,579\text{ cm}^{-1}$  can be assigned to the N–H in-plane bend modes. In addition, there are also strong bands at  $611$  and  $771\text{ cm}^{-1}$ , which can be assigned to C–C–C ring in-plane bend mode and C–H out-of-plane bend mode, correspondingly. The EF can be estimated as follows:  $EF = (I_{\text{SERS}}/I_{\text{bulk}})/(N_{\text{ads}}/N_{\text{bulk}})$  (Huang et al. 2009), where  $I_{\text{SERS}}$  is the intensity of a vibrational mode in the surface-enhanced spectrum,  $I_{\text{bulk}}$  is the intensity of the same mode in the Raman spectrum,  $N_{\text{bulk}}$  is the number of bulk molecules probed for a bulk sample, and  $N_{\text{ads}}$  is the number of molecules constituting the first monolayer adsorbed on the grating under the laser spot area. The Raman spectra of R6G solution (0.02 M) was used for the enhancement factor for the “bulk” values. The EF can be estimated with approximate calculation through monolayer–adsorbed mode (see Supporting Information) (Chang et al. 2012). The EF value for the C–C stretching at  $1,363\text{ cm}^{-1}$  of the R6G adsorbed on the Ag NPs–GE substrates as prepared was  $2.7 \times 10^5$ .

Figure 6B gives the SERS spectra of R6G adsorbed onto the Ag NPs–GE substrates as prepared with the weight ratio of AgAC: GO of 3:5, 4:5, 5:5, and 6:5, respectively. When the weight ratio of AgAC: GO was 3:5, the SERS spectrum of R6G is very weak (Fig. 6Ba), and with the weight ratio of AgAC: GO increased to 4:5 (Fig. 6Bb), the SERS intensity of R6G is remarkably higher in comparison with that of 3:5.

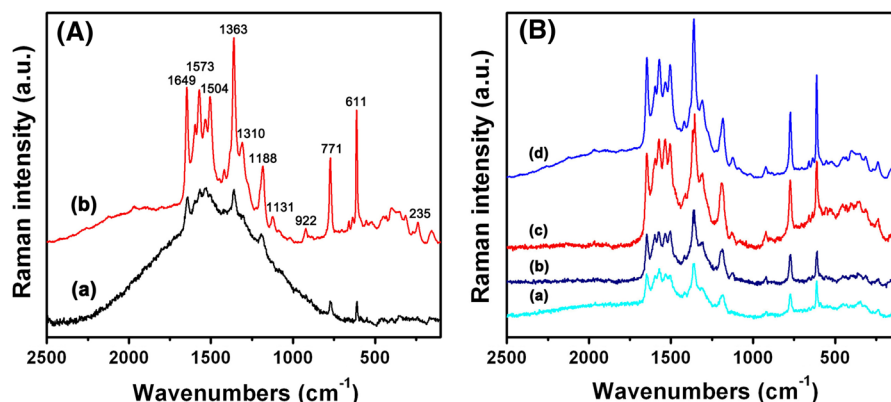


**Fig. 6** **A** Raman spectrum of 0.02 M R6G solution (a), SERS spectrum of R6G adsorbed on Ag NPs-GE substrate measured at 780 nm (b), **B** SERS spectra of R6G adsorbed on Ag NPs-GE

substrate fabricated with different AgAC: GO weight ratios: (a) 3:5, (b) 4:5, (c) 5:5, and (d) 6:5

The SERS intensity of R6G adsorbed on the Ag NPs-GE substrates is increasing with further increase of the weight ratio of AgAC: GO (Fig. 6Bc). However, with the weight ratio of AgAC: GO increased to 6:5, the SERS intensity did not increase obviously (Fig. 6Bd). The results show that the SERS activity of these substrates was greatly influenced by the loading amount of Ag NPs in the composites. According to the literature, we concluded that the increase of the Ag NPs can decrease the distance between the nanoparticles and the number of “hot spots” increase, which can improve the SERS activity of substrate (Sun et al. 2011). However, as the AgAC: GO ratio further increased, the Ag NPs terribly aggregated, which would deteriorate the SERS activity. The results are similar with the report of the influence of particle number on the hot spots in strongly coupled Ag NP chains (Wang et al. 2008).

One of the important issues here is why Ag NPs-GE substrate has high-SERS activity for R6G. We all know that it is difficult to obtain the Raman signals of high-concentrated R6G because of its strong fluorescence background (Fig. 6A). Meanwhile, it is also difficult to obtain the Raman signals of R6G with low concentration. Like pyridine, the R6G molecule has an ethylamino with positive charge. Therefore, the R6G molecules can be absorbed easily onto the surface of GE sheets by electrostatic attraction between positively charged ethylamino and negatively charged GE sheets. Importantly, for R6G adsorbed on GE, the fluorescence emission was weaker, which make the Raman peaks become clear (Xie et al. 2009). In

addition, R6G molecule has a nitrogen atom with a lone electron pair. Thus, the Ag-N can be formed through chemisorptive between ethylamino nitrogen atom and Ag NPs (Hildebrandt and Stockburger 1984). In view of Fig. 6Bb, a new and strong peak can be found at ca. 235 cm<sup>-1</sup>, which can be assigned to Ag-N band. Indeed, many amino acids chemisorbed to Ag shows Ag-N vibrations in the range of 220–240 cm<sup>-1</sup> (Venekatesan et al. 1980). The results showed that the Ag NPs-GE substrates with high-SERS activity give a great promise for SERS application.

The size of Ag NPs has important effect on the SERS activity. To the best knowledge of us, the optimum size of Ag NPs for SERS activity is around 100 nm, and when the size is below 100 nm, the SERS signal increases with an increase of the size (Zhou et al. 2011). Herein, average particle size of Ag NPs about 45, 65, and 88 nm can be obtained after thermal treating at 300, 500, and 700 °C, correspondingly, as shown in Fig. 7. The same phenomenon was found as shown in Fig. 7d that the SERS activity of the films really increased with the increasing of the average particle size of Ag NPs. We cannot further increase the particle size simply by increase the annealing temperature because of the unavoidable aggregation (see Fig. S4 in supplementary information). To investigate the influence of particle size on the SERS activity in detail, different preparation procedures should be designed, which have been carried out in our lab, and the results would be published elsewhere.



**Fig. 7** Typical SEM images of Ag NPs–GE film treated under temperatures of 300 °C (a), 500 °C (b), and 700 °C (c); The SERS spectra of CV ( $1 \times 10^{-6}$  M) adsorbed onto the Ag NPs–GE with annealing under different temperatures, and the Raman spectrum of CV solid was used for comparison

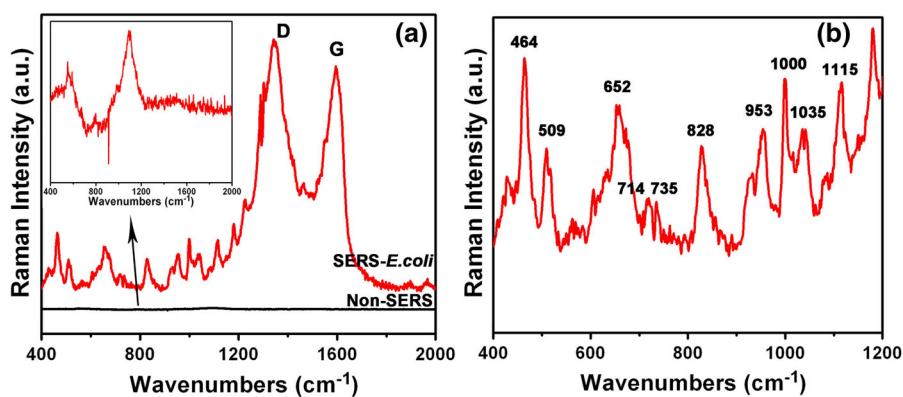
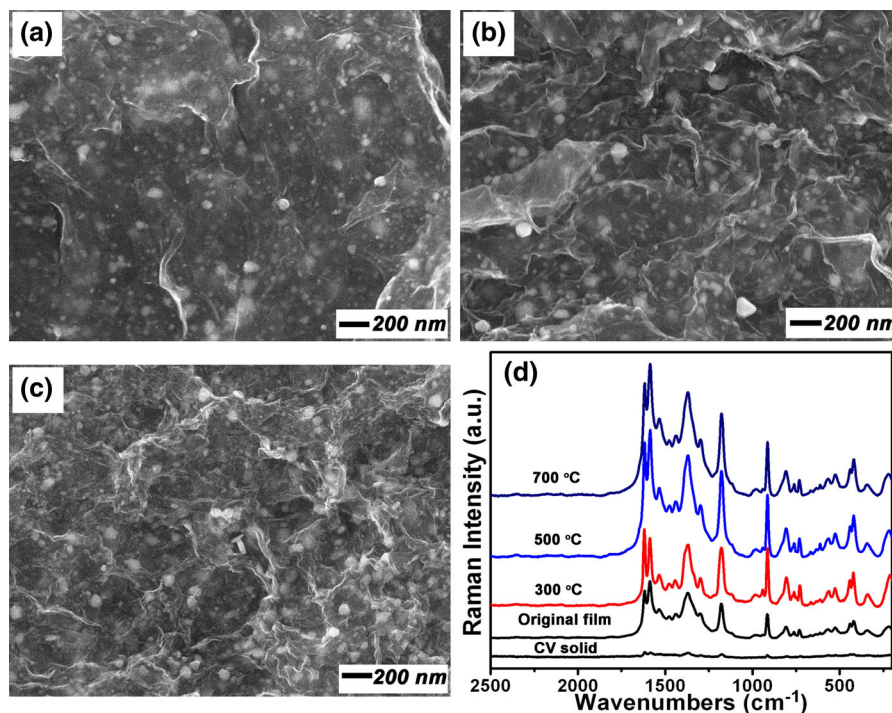


**Fig. 8** **a** SERS spectrum of *E. coli* cell onto the Ag NPs–GE film and non-SERS spectrum sample placed onto the glass; **b** SERS spectrum of *E. coli* in the range of wavenumbers from 400 to 1,200  $\text{cm}^{-1}$

The ability to provide a unique vibrational signature of a biologically or medically relevant species lacking any visible chromophores in aqueous solution at low concentrations illustrates the potential that SERS is a valuable analytical and structural spectroscopic tool. In particular, the development of SERS for the detection and identification of bacterial pathogens has attracted recent research interest motivated by both applications in clinical diagnostic microbiology

and the current heightened concerns about potential bioterrorist attacks. Here, the application of our as-prepared SERS substrate in detecting of bacterial cell such as *E. coli* was discussed. The observed corresponding SERS and non-SERS spectra of *E. coli* are compared in Fig. 8a. In the non-SERS spectrum, no vibrational band can be observed. Through amplifying the intensity, only a vibrational band at 1,090  $\text{cm}^{-1}$  can be found. However, in the SERS spectrum,

vibrational bands at 464, 509, 652, 714, 735, 828, 953, 1,000, 1,035, and 1,115  $\text{cm}^{-1}$  appeared, which indicated the excellent SERS property of our SERS substrate (Fig. 8b). Actually, some reports have demonstrated the Raman spectrum of *E. coli* (Guzelian et al. 2002; Premasiri et al. 2005; Jarvis and Goodacre 2004). Although many of the same vibrational bands appeared in the SERS spectra of *E. coli* reported here and by Guzelian et al. (2002), the most intense features were at 714 and 1,132  $\text{cm}^{-1}$ , 732 and 1,027  $\text{cm}^{-1}$  in the Premasiri's work (2005) and only one intense feature at 652  $\text{cm}^{-1}$  can be found in Goodacres work (2004). But in our spectrum, all the vibrational bands reported are observed, and some vibrational bands have not been reported in previous studies such as at 464, 509, 828, and 953  $\text{cm}^{-1}$  also can be found. This special result indicated the excellent SERS activity toward *E. coli* which encourages us to continue this work in the future.

## Conclusions

The Ag NPs–GE composite has been prepared, where the Ag NPs with an average diameter of 22 nm were assembled to the GE sheets through the solvothermal method using GO sheets as substrates and the hydrazine hydrate as a reducing agent. Then, through the vacuum filtration, the Ag NPs–GE film can be obtained. The high SERS-active of Ag NPs makes a significant contribution to the high sensitivity of SERS to R6G molecules with an EF of  $2.7 \times 10^5$ . The results demonstrated that the degree of Ag NPs in GE sheets is a very important factor determining the magnitude of SERS signal enhancement and the sensitivity of detection. The as-prepared substrate shows good SERS sensitivity to *E. coli*. The high sensitivity, large-scale, cheap, and free-standing features are integrated in the obtained substrates. What's more, they are easily handled and disposable, which would bring a great convenience to the routine SERS detection.

**Acknowledgments** This work was supported by the National Science Foundation of China (50902061, 51302113), Six Personnel Peak Project (2009137) of Jiangsu Province, Scientific and Technical Innovation Project for Graduate Students (CXZZ12\_0670, CXZZ13\_0664) and Undergraduate Students of Jiangsu Province (201313986004Y). Excellent Ph.D training program in Jiangsu University (1141220014). Students

research project in Jiangsu University (12A299). Supported by the Opening Project of Key Laboratory of Soft Chemistry and Functional Materials (Nanjing University of Science and Technology), Ministry of Education, China.

## References

- Abu Hatab NA, Oran JM, Sepaniak MJ (2008) Surface-enhanced Raman spectroscopy substrates created via electron beam lithography and nanotransfer printing. *ACS Nano* 2:377–385
- Albrecht MG, Creighton JA (1977) Anomalous intense Raman spectra of pyridine at a silver electrode. *J Am Chem Soc* 99:5215–5217
- Chang CC, Yang KH, Liu YC et al (2012) Surface-enhanced Raman scattering-active Au/SiO<sub>2</sub> nanocomposites prepared using sonoelectrochemical pulse deposition methods. *ACS Appl Mater Interfaces* 4:4700–4707
- Dikin DA, Stankovich S, Zimney EJ (2007) Preparation and characterization of graphene oxide paper. *Nature* 448:457–460
- Fleischmann M, Hendra PJ, McQuillan AJ (1974) Raman spectra of pyridine adsorbed at a silver electrode. *Chem Phys Lett* 26:163–166
- Fu XQ, Bei FL, Wang X et al (2009) Surface-enhanced Raman scattering of 4-mercaptopyridine on submonolayers of  $\alpha$ -Fe<sub>2</sub>O<sub>3</sub> nanocrystals (sphere, spindle, cube). *J Raman Spectrosc* 40:1290–1295
- Fu XQ, Bei FL, Wang X et al (2010) Surface-enhanced Raman scattering of silylated graphite oxide sheets sandwiched between colloidal silver nanoparticles and silver piece. *J Raman Spectrosc* 41:370–373
- Guzelian AA, Sylvia JM, Janni JA et al (2002) SERS of whole-cell bacteria and trace levels of biological molecules. *Proc SPIE* 4577:182
- Hasell T, Lagonigro L, Peacock AC et al (2008) Silver nanoparticle impregnated polycarbonate substrates for surface enhanced Raman spectroscopy. *Adv Funct Mater* 18:1265–1271
- He D, Hu B, Yao QF et al (2009) Large-scale synthesis of flexible free-standing SERS substrates with high sensitivity: Electrospun PVA nanofibers embedded with controlled alignment of silver nanoparticles. *ACS Nano* 3:3993–4002
- Hildebrandt P, Stockburger M (1984) Surface-enhanced resonance Raman spectroscopy of rhodamine 6G adsorbed on colloidal silver. *J Phys Chem* 88:5935–5944
- Huang GG, Han XX, Hossain MK et al (2009) Development of a heat-induced surface-enhanced Raman scattering sensing method for rapid detection of glutathione in aqueous solutions. *Anal Chem* 81:5881–5888
- Hummers WS, Offeman RE (1958) Preparation of graphitic oxide. *J Am Chem Soc* 80:1339–1339
- Jarvis RM, Goodacre R (2004) Discrimination of bacteria using surface-enhanced Raman Spectroscopy. *Anal Chem* 76:40–47
- Jeanmaire DL, VanDuyne RP (1977) Surface Raman spectro-electrochemistry: Part 1. Heterocyclic, aromatic, and aliphatic amines adsorbed on the anodized silver electrode. *J Electroanal Chem* 84:1–20
- Kim K, Shin D, Kim KL et al (2012) Surface-enhanced Raman scattering of 4,4'-dimercaptoazobenzene trapped in Au nanogaps. *Phys Chem Chem Phys* 14:4095–4100

- Kneipp K, Kneipp H, Itzkan I et al (1999) Ultrasensitive chemical analysis by Raman spectroscopy. *Chem Rev* 99:2957–2975
- Kneipp K, Kneipp H, Corio P et al (2000) Surface-enhanced and normal stokes and anti-stokes Raman spectroscopy of single-walled carbon nanotubes. *Phys Rev Lett* 84:3470–3473
- Kudin KN, Ozbas B, Schniepp HC et al (2008) Raman spectra of graphite oxide and functionalized graphene sheets. *Nano Lett* 8:36–41
- Lu F, Zhang SH, Gao HJ et al (2012) Protein-decorated reduced oxide graphene composite and its application to SERS. *ACS Appl Mater Interfaces* 4:3278–3284
- Murphy S, Huang L, Kamat PV (2013) Reduced graphene oxide-silver nanoparticle composite as an active SERS material. *J Phys Chem C* 117:4740–4747
- Premasiri WR, Moir DT, Klempner MS et al (2005) Characterization of the surface enhanced Raman scattering (SERS) of bacteria. *J Phys Chem B* 109:312–320
- Sun LL, Zhao DX, Ding M et al (2011) Controllable synthesis of silver nanoparticle aggregates for surface-enhanced Raman scattering studies. *J Phys Chem C* 115:16295–16304
- Venekatesan S, Erdheim G, Lombardi JR et al (1980) Voltage dependence of the surface-molecule line in the enhanced Raman spectrum of several nitrogen containing compounds. *Surf Sci* 101:387
- Wang ZB, Luk'yanchuk BS, Guo W et al (2008) The influences of particle number on hot spots in strongly coupled metal nanoparticles chain. *J Chem Phys* 128:094705
- Xie L, Ling X, Fang Y et al (2009) Graphene as a substrate to suppress fluorescence in resonance Raman spectroscopy. *J Am Chem Soc* 131:9890–9891
- Xu C, Wang X (2009) Fabrication of flexible meral-nanoparticle films using graphene oxide sheets as substrates. *Small* 5:2212–2217
- Yang J, Zang CL, Sun L et al (2011) Synthesis of graphene/Ag nanocomposite with good dispersibility and electroconductibility via solvothermal method. *Mater Chem Phys* 129:270–274
- Zhou HQ, Qiu CY, Yu FH et al (2011) Thickness-dependent morphologies and surface-enhanced Raman scattering of Ag deposited on n-layer graphenes. *J Phys Chem C* 115:11348–11354